



ORIGINAL ARTICLE

Zeolite framework silicon allotropes with direct band gap



Yanxing Song^{a,*}, Changchun Chai^a, Qingyang Fan^{b,*}, Wei Zhang^a, Yintang Yang^a

^a State Key Discipline Laboratory of Wide BandGap Semiconductor Technology, School of Microelectronics, Xidian University, Xi'an, People's Republic of China

^b School of Information and Control Engineering, Xi'an University of Architecture and Technology, Xi'an, People's Republic of China

Received 8 June 2022; accepted 18 October 2022

Available online 25 October 2022

KEYWORDS

Zeolite framework;
Silicon allotrope;
Direct band gap semiconductor;
Optical absorption;
Effective mass

Abstract It is a significant issue in the field of semiconductor devices and optoelectronic devices to find silicon allotropes with high mobility, direct band gap and high light absorption to replace traditional diamond silicon (d-Si). By constructing a zeolite framework, fifteen silicon allotropes with a direct band gap of 0.47–1.66 eV were screened from hundreds of zeolite framework silicon allotropes by ab initio calculations. The crystal structures, stability, effective mass, mechanical, electronic and optical properties were comprehensively studied. Compared with diamond silicon, several allotropes showed easy doping, low carrier effective mass and high absorption of the solar spectrum, which indicate promising candidates for adoption in photovoltaic applications.

© 2022 The Author(s). Published by Elsevier B.V. on behalf of King Saud University. This is an open access article under the CC BY-NC-ND license (<http://creativecommons.org/licenses/by-nc-nd/4.0/>).

1. Introduction

Although second- and third-generation semiconductors have been proposed for many years, silicon still have wide range of applications in the field of microelectronics and photovoltaic power due to its abundance mature technology. However, the indirect band gap with low solar absorptivity limits its potency in future photovoltaic applications. Although many new materials have been proposed to replace silicon, small natural reserves and high synthetic costs limit their application at the industry level. The ideal solution is to engineer silicon such that

it gets qualitative leap in solar absorption. Therefore, amount of works has been done to design, discover and synthesize a direct bandgap novel silicon phase with improved absorption properties.

Silicon retains its diamond (Si-I) structure up to ~ 11.7 GPa. It has several metastable phases under pressure that are stable (Mujica et al., 2003). As the pressure rises, the metallic β -tin phase (Si-II), Orthorhombic *Imma* phase, hexagonal phase (Si-V), hexagonal close-packed phase (hcp) and orthorhombic *Cmca* phase (Si-VI) are formed successively. A face-centered cubic crystal is synthesized that remains stable up to pressure of ~ 250 GPa. Under pressure release starting from the β -tin phase, the R8 (Si-XII), BC8 (Si-III), hexagonal diamond phase (Si-IV), *Ibam* phase (Si-IX) and ST-12 phase have been observed successively (Jamieson 1963, Besson et al., 1987, Ackland 2001, Malone et al., 2008, Malone et al., 2008, Wippermann et al., 2016). However, they are unsuitable for solar cells since they are either metallic (all phases above 12 GPa), semi-metallic (BC8), or have a band gap that is indirect (1 eV for Si-IV) or too small (0.24 eV for R8).

Although the breakthrough of silicon allotropes in photoelectric applications has not been achieved experimentally, it indicates the feasibility of silicon allotrope design. Botti et al. predicted several low-

* Corresponding authors.

E-mail addresses: syx739686768@163.com (Y. Song), qyfan_xidian@163.com (Q. Fan).

Peer review under responsibility of King Saud University.



energy phases of silicon with quasi-direct gaps from 1.0 to 1.5 eV (Botti et al., 2012). Amsler et al. discovered a plethora of low-energy and low-density silicon allotropes with cage-like polyhedral and channel-like structures in which 11 structures are direct band gap semiconductors between 1.08 eV and 1.87 eV (Amsler et al., 2015). Through the comprehensive investigation of dynamic stability, thermodynamic stability and mechanical stability, researchers have reported a variety of possible silicon allotropes. For example, Wang et al predicted six direct band gap silicon allotropes with gap of 0.39–1.25 eV (Wang et al., 2014). Guo et al. proposed a new phase, $P6_3mmc$ Si₆, with a 0.64 eV direct gap and great optical properties (Guo et al., 2015). Furthermore, $Amm2$ -Si₂₀ (quasi-direct gap of 0.742 eV), Pm -Si₃₂ (direct gap of 1.85 eV), and $P2_1/m$ -Si₁₀ (direct gap of 0.83 eV) were predicted by Fan et al. (Fan et al., 2015, Fan et al., 2016). Comprehensive investigations showed that most silicon allotropes with a direct band gap perform better than diamond silicon in optical absorption, especially at visible wavelengths. Recently, Hu et al. predicted a silicon phase named Fvs-Si₄₈ by the property-selected genetic algorithm from the Reticular Chemistry Structure Resource (RCSR) (O’Keeffe et al., 2008) database (Hu et al., 2018). Wei et al. predicted six direct band gap silicon phases through the atomic substitution in known carbon structures (Wei et al., 2019). Furthermore, Zhang et al. predicted an indirect band gap allotrope that can be controlled to a direct gap at a strain of approximately 8 %, and the photon absorption can be tuned over a wide range of energies (Zhang et al., 2021). Random sampling strategy combined with space group and graph theory (RG²) code with space group and graph theory is also used widely to generate novel crystal phases (Shi et al., 2018). Silicon phase with direct band gap and quasi indirect band gap (He et al., 2018, Yang et al., 2018), topological nodal-line semimetal (Su et al., 2022) and other low energy materials with great optical absorption have been predicted successfully by RG² code (Jiao et al., 2019, Ouyang et al., 2020, Wei et al., 2022). Open-framework silicon allotrope is another all-silicon solid with potential applications in optoelectronic technologies. The Na₄Si₂₄ clathrate is synthesized by mixing powder Si and element Na for 1:6 under high temperature and pressure, and an all-silicon structure can be formed by removing the Na element from the clathrate. Thomas et al. studied this process (Shiell and Strobel 2020), and Guerette et al. realized the synthesis of 99.9985 % $Cmcm$ -Si₂₄ (Guerette et al., 2020). $Cmcm$ -Si₂₄ turned out to be a 1.4 eV quasi-direct band gap semiconductor. At the same time, because there are many cavities in open framework silicon allotropes, it is feasible to inject new elements into the allotropes to adjust their properties (Fix et al., 2020). $Cmcm$ -Si₂₄ present the same structure characteristics with the zeolite type CAS in the International Zeolite Association (IZA) database (Baerlocher et al., 2007), the pioneering synthesis of $Cmcm$ -Si₂₄ has highlighted the potential of developing novel silicon phase with zeolite framework.

In this paper, we generate hundreds of open-framework Si allotropes with sp^3 hybrid and large cavities by RG² code (Shi et al., 2018). After screening these open-framework silicon structures, we identify 15Si allotropes with zeolite framework and a direct band gap of 0.47–1.66 eV. These allotropes maintain the low-density characteristics of the zeolite and exhibit excellent transport and optical properties. All structures exhibit dynamic stability, thermodynamic stability and mechanical stability. To ensure the accuracy of the electronic properties, all band structure and optical property calculations adopt the HSE06 functional (Krukau et al., 2006).

2. Method

All calculations were performed using Medea Vienna ab initio simulation package (Medea-VASP) with density functional theory. The Perdew-Burke-Ernzerhof (PBE) exchange–correlation functional of the generalized gradient approximation (GGA) was adopted (Hohenberg and Kohn 1964, Kohn and Sham 1965, Hafner 2008). The spacing of k -points was

0.2 \AA^{-1} , and the energy cut-off of the plane wave was set to 360 eV. The convergence criteria for electron optimization and ionic relaxation were set to be no more than 1×10^{-7} eV and 2×10^{-2} eV/Å, respectively. The HSE06 hybrid functional with 34 % exact exchange energy is applied in optical and band structure calculations to overcome the band gap underestimation (Krukau et al., 2006). In effective mass calculations, to obtain the Hessian matrix of E - k (Effective mass tensor [m^{-1} ij]), we divide a $9 \times 9 \times 9$ k-point grid around the band edge with each k point is 0.0005 Bohr^{-1} apart (Song et al., 2020). The phonon spectra were calculated by the Phonopy code with the density functional perturbation theory (DFPT) for $3 \times 3 \times 3$ supercell (Stefano et al., 2001, Togo and Tanaka 2015).

3. Results and discussion

3.1. Structural properties

According to the structural characteristics, the silicon allotropes are named using their corresponding zeolite framework types: ACO-Si₁₆ ($IM-3 M$), AEI-Si₄₈ ($CMCM$), AFX-Si₄₈ ($P6_3/MMC$), ANA-Si₄₈ ($IA-3D$), BOZ-Si₉₂ ($CMCM$), BPH-Si₂₈ ($P-62 M$), EDI-Si₅ ($P-4 M2$), ETR-Si₄₈ ($P6_3MC$), GME-Si₂₄ ($P6_3/MMC$), LEV-Si₅₄ ($R-3 M$), LIT-Si₂₄ ($PNMA$), MEL-Si₉₆ ($I-4 M2$), RWR-Si₃₂ ($I41/AMD$), SAT-Si₇₂ ($R-3 M$) and SGT-Si₆₄ ($I41/AMD$). The schematic representation of the zeolite framework silicon allotropes is shown in Fig. 1, and the cages with the same color present that they have the same symmetry of space translation. All of the allotropes are composed of several large cages or open channels with sp^3 bonding. Among them, ACO-Si₂₄ was predicted by replacing the atoms with silicon in the known carbon allotropes, and we now classify it into a zeolite framework (Wei et al., 2019). The lattice parameters are listed in Table 1, and the Wyckoff positions are shown in Table S1. Our calculated lattice constants of diamond phase and ACO-Si₂₄ are in good agreement with the experimental value and those of reported work, respectively, indicating a suitable choice of method and parameters in our calculations.

The enthalpy of these silicon allotropes relative to diamond phase was calculated using the formula $\Delta H = E_{\text{allotrope}}/n_1 - E_{\text{diamond}}/n_2$, where n_1 and n_2 are the number of silicon atoms per cell of allotropes and diamond phase, respectively. Fig. 2 shows the calculated relative enthalpy as a function of mass density for all zeolite allotropes and diamond silicon. Among the allotropes, LIT-Si₂₄, MEL-Si₉₆ and SGT-Si₆₄ are the most stable, with approximately 0.127 eV/atom higher enthalpy than diamond silicon at ambient conditions, while the highest energy allotrope is BOZ-Si₉₂, which is 0.671 eV/atoms higher than d-Si. On the whole, the relative enthalpy for zeolite framework silicon allotropes is inversely proportional to the mass density. BOZ-Si₉₂ shows the lowest density of 1.195 g/cm³, which is close to water (1.0 g/cm³). All allotropes are lighter than diamond silicon due to their open framework with a large cavity. The thermal stability of most allotropes except BOZ-Si₉₂, EDI-Si₅ and ETR-Si₄₈ are better than the reported t-Si₆₄ with relative enthalpy of 0.408 eV/atoms (Fan et al., 2019). The phonon dispersions of BOZ-Si₉₂, EDI-Si₅ and ETR-Si₄₈ are shown in Fig. 2, and other allotropes are shown

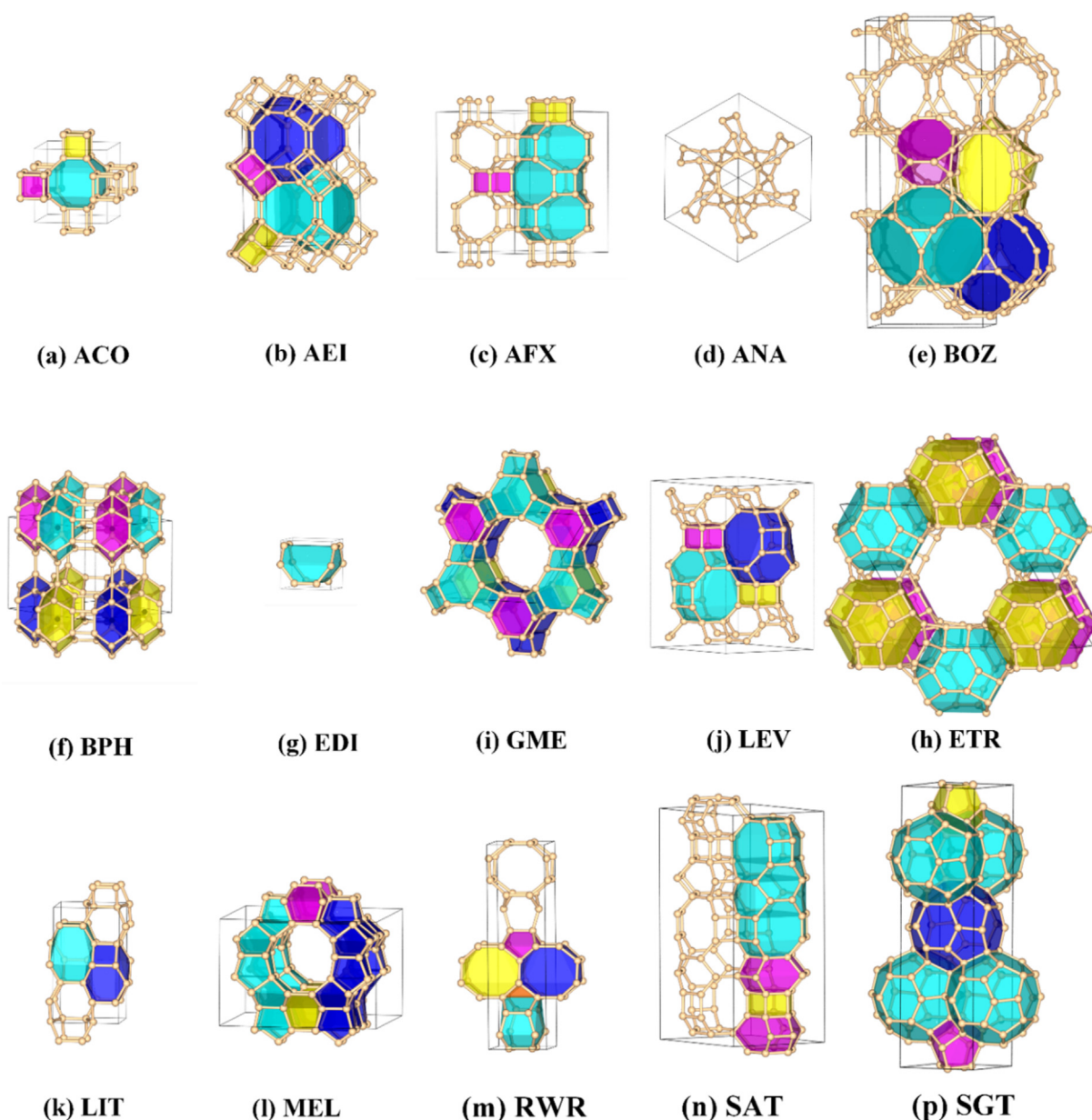


Fig. 1 Structures of zeolite framework silicon allotropes. Polyhedral cages that constitute building blocks for crystal lattice of silicon allotropes are presented in different color.

in Fig. S1. All predicted novel zeolite framework silicon allotropes are proved to be dynamic stability.

3.2. Mechanical properties

The mechanical properties and mechanical stability of zeolite framework allotropes were also investigated thoroughly. ACO-Si₂₄ and ANA-Si₄₈ belong to the cubic system that have 3 independent elastic stiffness constants. AEI-Si₄₈, BOZ-Si₉₂ and LIT-Si₂₄ belong to orthorhombic system that have 9 independent elastic stiffness constants. AFX-Si₄₈, BPH-Si₂₈, ETR-Si₄₈ and GME-Si₂₄ belong to the hexagonal system that have 5 independent elastic stiffness constants. EDI-Si₅, MEL-Si₉₆, RWR-Si₃₂ and SGT-Si₆₄ belong to the tetragonal system that have 6 independent elastic stiffness constants. LEV-Si₅₄ and

SAT-Si₇₂ belong to the trigonal system that have 6 independent elastic stiffness constants. The strain-energy method is adopted in elastic calculations, and the results are listed in Table 2. For comparison, diamond silicon is investigated using the same method. The positive definite of the stiffness matrix indicate that all these zeolite framework silicon allotropes are mechanically stable.

Elastic moduli are important indexes to measure the strain behavior of crystal. We investigated zeolite framework silicon allotropes from the perspective of isotropic polycrystalline approximation and single crystals. Voigt-Ruess-Hill (VRH) approximation is adopted to represent the elastic behavior of polycrystalline materials. Voigt and Ruess proposed the upper limits and lower limits of the bulk modulus B and shear modulus G , respectively. Hill gives an arithmetic average of Voigt's

Table 1 Crystal lattice parameters, mass density and relative enthalpy of diamond silicon and zeolite framework silicon allotropes.

	Space Group	a (Å)	b (Å)	c (Å)	γ (°)	Density (g/cm ³)	Relative enthalpy (eV/atom)
ACO	<i>IM-3 M</i>	7.496	7.496	7.496	90	1.77	0.30
AEI	<i>CMCM</i>	10.488	9.652	14.094	90	1.56	0.33
AFX	<i>P63/MMC</i>	10.543	10.543	14.776	120	1.57	0.32
ANA	<i>IA-3D</i>	10.347	10.347	10.347	90	2.02	0.24
BOZ	<i>CMCM</i>	11.194	29.571	10.850	90	1.19	0.67
BPH	<i>P-62 M</i>	10.185	10.185	10.012	120	1.45	0.34
EDI	<i>P-4 M2</i>	5.252	5.252	4.924	90	1.71	0.51
ETR	<i>P63MC</i>	16.287	16.287	6.559	120	1.48	0.40
GME	<i>P63/MMC</i>	10.526	10.526	7.481	120	1.55	0.32
LEV	<i>R-3 M</i>	9.948	9.948	17.569	120	1.67	0.28
LIT	<i>PNMA</i>	11.776	6.749	6.677	90	2.10	0.12
MEL	<i>I-4 M2</i>	15.358	15.358	10.345	90	1.83	0.12
RWR	<i>I41/AMD</i>	5.942	5.942	20.846	90	2.02	0.16
SAT	<i>R-3 M</i>	9.758	9.758	23.549	120	1.72	0.26
SGT	<i>I41/AMD</i>	7.815	7.815	26.672	90	1.83	0.12
Diamond-Si	<i>FD-3 M</i>	5.456	5.456	5.456	90	2.32	0
Diamond-Si ^a	<i>FD-3 M</i>	5.431			90	2.33	
ACO ^b	<i>IM-3 M</i>	7.494			90	1.77	0.32

^a (Song et al., 2019) ^b (Wei et al., 2019).

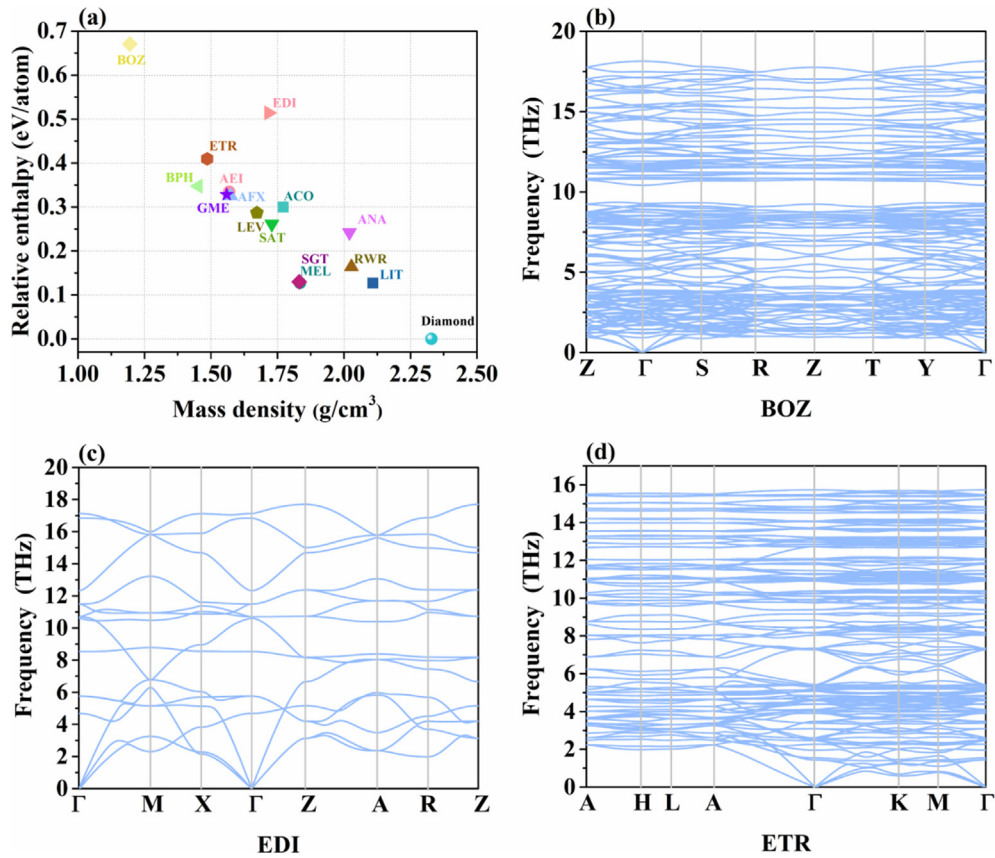


Fig. 2 (a) Relative enthalpy as a function of mass density for all optimized zeolite framework silicon allotropes. (b-d) Phonon spectra of BOZ-Si₉₂, EDI-Si₅ and ETR-Si₄₈.

Table 2 Calculated elastic constants (GPa), elastic modulus (GPa), Poisson's ratio and band gap (eV) of zeolite framework silicon allotropes and diamond silicon.

Zeolite framework	C_{11}	C_{22}	C_{33}	C_{44}	C_{55}	C_{66}	C_{12}	C_{13}	C_{23}	C_{14}	B	E	G	V	B/G	E_g
ACO	82	82	82	31	31	31	50	50	50	0	60	63	24	0.33	2.54	0.66
AEI	82	70	83	13	16	29	45	31	29	0	49	51	19	0.33	2.58	1.31
AFX	84	84	49	24	24	22	41	40	40	0	49	50	19	0.33	2.54	1.19
ANA	123	123	123	40	40	40	40	40	40	0	68	101	40	0.25	1.69	1.55
BOZ	38	54	45	10	13	9	24	15	25	0	29	30	11	0.33	2.55	0.47
BPH	65	65	81	11	11	15	35	23	23	0	41	40	15	0.34	2.73	1.04
EDI	133	133	134	14	14	7	15	23	23	0	58	60	22	0.33	2.58	1.36
ETR	51	51	69	11	11	15	21	21	21	0	33	38	14	0.31	2.29	1.26
GME	82	82	55	23	23	23	37	39	39	0	49	53	20	0.32	2.46	0.80
LEV	78	78	83	24	24	21	36	46	46	-0.6	55	56	21	0.33	2.60	1.35
LIT	158	106	142	30	51	39	47	51	43	0	75	104	41	0.27	1.84	1.00
MEL	118	118	119	30	30	22	28	40	40	0	63	82	32	0.28	1.99	1.56
RWR	155	155	142	34	34	40	37	38	38	0	75	108	43	0.26	1.75	1.09
SAT	93	93	110	26	26	27	39	33	33	2.1	56	72	28	0.29	1.99	0.61
SGT	123	123	125	34	34	31	35	35	35	0	64	94	37	0.26	1.73	1.66
Diamond Si	152			75			57				89	152	62	0.22	1.44	

and Reuss's definitions. Young's modulus E and Poisson's ratio ν of polycrystalline are obtained using: (Fan et al., 2021).

$$E = \frac{9BG}{3B + G} \quad (1)$$

$$\nu = \frac{3B - 2G}{2(3B + G)} \quad (2)$$

The calculated moduli, Poisson's ratio and B/G ratio of the allotropes are listed in Table 2. Young's modulus and shear modulus represents the ability of a crystal against linear and shear deformation, respectively. A higher Poisson's ratio usually gives a better plasticity. The calculated moduli of the allotropes are lower than those of diamond silicon, while all allotropes have a higher Poisson's ratio than diamond silicon, indicating that zeolite framework silicon allotropes are more plastic than diamond Si but are less resistant to strain. Among the allotropes, ANA-Si₄₈, LIT-Si₂₄ and RWR-Si₃₂ present a higher moduli, indicating that they have higher mechanical strength. Other structures with a lower elastic modulus and larger Poisson's ratio present foreseeable ductility. ACO-Si₂₄, AEI-Si₄₈, AFX-Si₄₈, BOZ-Si₉₂, BPH-Si₂₈ and EDI-Si₅ have a similar Poisson's ratio ν of 0.33. Moreover, the ratio of the B and G identify the brittle or ductile of crystals (Fan et al., 2022). If B/G greater than 1.75, then the crystal manifests ductile features; otherwise, it manifests brittle features. Most allotropes show ductility, which is consistent with Poisson's ratios. ANA-Si₄₈ ($B/G = 1.69$) and SGT-Si₆₄ ($B/G = 1.73$) exhibit brittle features but are still higher than diamond silicon ($B/G = 1.43$).

For a single crystal, different crystallographic plane with different periodicities lead to different chemical and physical properties. Young's modulus anisotropy plays a significant role in crystal physics. The direction dependent Young's modulus is obtained by the following equations:

$$\begin{aligned}
1/E(n) = & S_{11}n_1^4 + S_{22}n_2^4 + S_{33}n_3^4 + (S_{44} + 2S_{23})n_2^2n_3^2 \\
& + (S_{55} + 2S_{31})n_3^2n_1^2 + (S_{66} + 2S_{12})n_1^2n_2^2 \\
& + 2n_2n_3[(S_{14} + S_{56})n_1^2 + S_{24}n_2^2 + S_{34}n_3^2] \\
& + 2n_3n_1[S_{15}n_1^2 + (S_{25} + S_{46})n_2^2 + S_{35}n_3^2] \\
& + 2n_1n_2[(S_{16}n_1^2 + S_{26}n_2^2 + (S_{34} + S_{45})n_3^2]
\end{aligned} \quad (3)$$

where the n_1 , n_2 and n_3 , are the direction cosine and S_{ij} are the elastic compliance constants of crystals. Three-dimensional surfaces are adopted to investigate the Young's moduli anisotropy of all the zeolite framework allotropes, and the results are shown in Fig. 3. Most of the allotropes show degrees of anisotropy to different extents except ANA-Si₄₈. ANA-Si₄₈ is a mechanical isotropous crystal that is unusual. In Fig. 3, the magenta and cyan colors represent the highest and lowest Young's moduli of the allotropes, respectively. It is obvious that EDI-Si₅ has the largest anisotropy of Young's modulus with maximum and minimum values of 129 GPa and 25 GPa, respectively.

3.3. Electronic properties

The band structures were calculated at the hybrid functional HSE06 to overcome the underestimated band gaps of the standard PBE functional. As shown in Fig. 4, the screened zeolite framework silicon allotropes are all direct band gap semiconductors. Among allotropes, the largest band gap is found in SGT-Si₆₄, indicating that the direct gap zeolite framework allotropes of silicon have great potential as photovoltaic materials. BOZ-Si₉₂ with a 0.47 eV direct band gap shows a strong ability to capture low-energy photons, which is promising in tandem solar cell applications. The effective mass is a key parameter for carrier mobility, which characterizes the conductive properties of materials. Furthermore, the atomic orbitals have been projected in band structures, the s orbital is the major contributor to the conduction band minimum (CBM) of allotropes and the valence band maximum (VBM) is mainly contributed by p orbitals. For the VBM of these allotropes, the BPH is mainly contributed by the p_x orbital, and AEI-Si₄₈, AFX-Si₄₈, GME-Si₂₄, LEV-Si₅₄, LIT-Si₂₄, RWR-Si₃₂ and SAT-Si₇₂ are mainly contributed by the p_z orbital. The VBM of other crystals is contributed by all the p_x , p_y and p_z orbitals. The effective mass of the carriers depends on the electronic state at the edge of the band, which is defined as:

$$E(\vec{k}) = E(\vec{k}_0) \pm \frac{\hbar^2}{2} [\vec{k} - \vec{k}_0] [m_i^{-1}] [\vec{k} - \vec{k}_0]^T \quad (4)$$

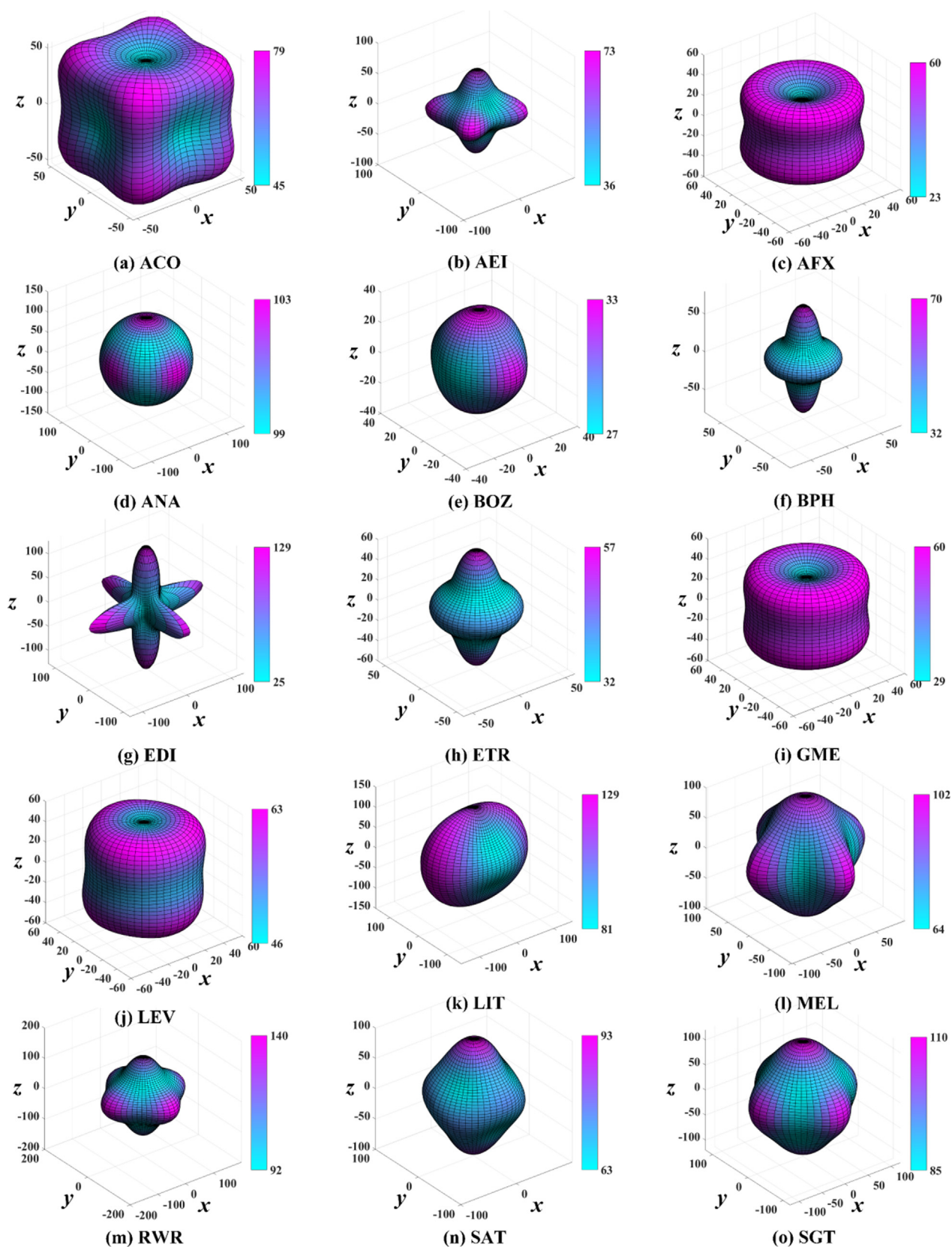


Fig. 3 Directional dependence of Young's modulus (GPa) for zeolite framework silicon allotropes. Magenta and cyan colors represent highest and lowest Young's moduli of allotropes, respectively.

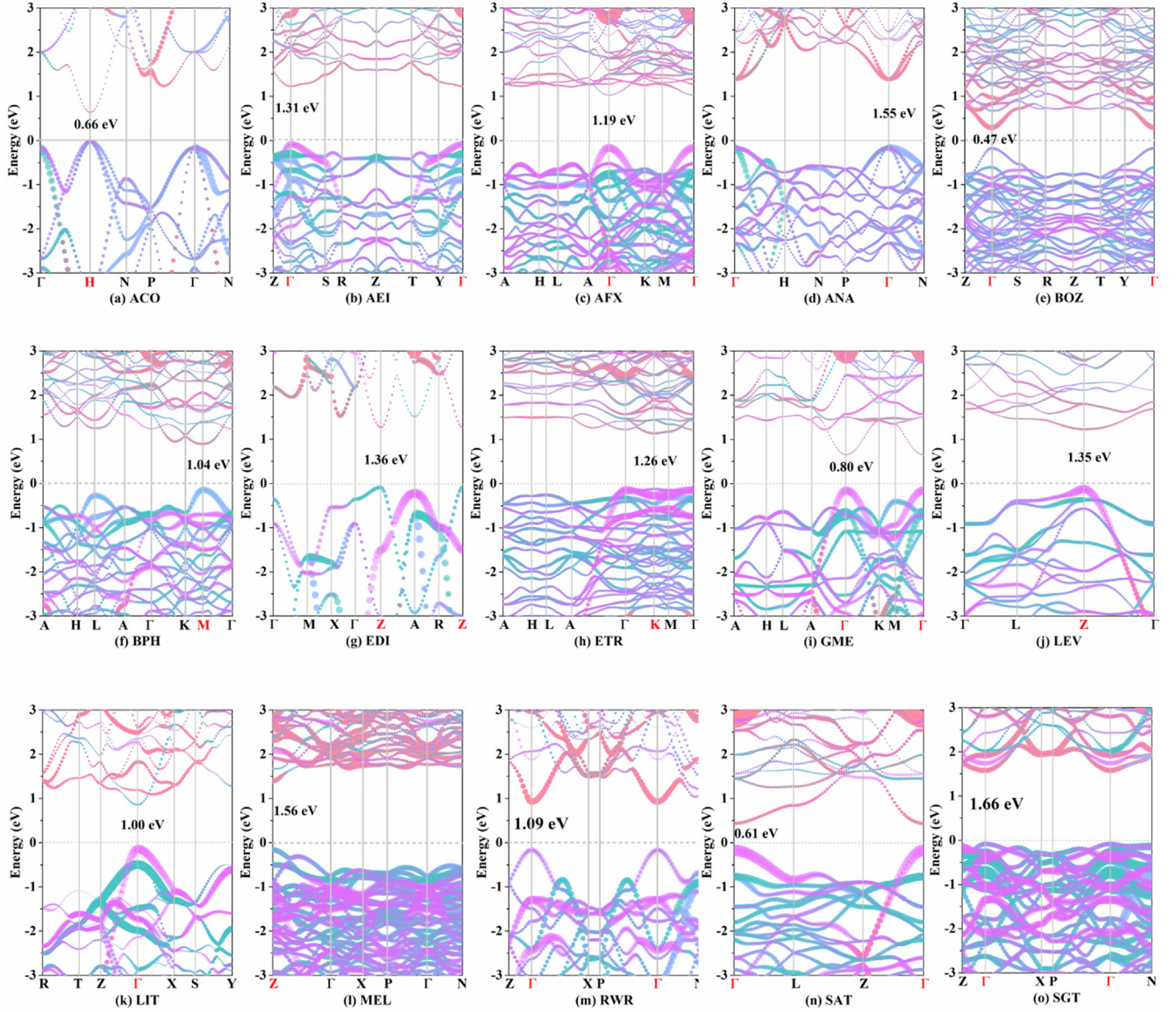


Fig. 4 Electronic band structures. Sizes of pink, light blue, dark cyan and light magenta circles represent projected weights of Si s , Si p_x , Si p_y and Si p_z orbitals, respectively. Position in first Brillouin zone of direct gap is marked in red.

where \hbar is the reduced Planck constant, and $E(\vec{k}_0)$ represents the energy eigenvalues at the band edge. $[m^{-1}]_{ij}$ is the Hessian matrix of $E-k$ at k_0 which called the effective mass tensor. The direction dependent effective mass is calculated by:

$$\frac{1}{m^*} = [n_1 \ n_2 \ n_3][m_{ij}^{-1}][n_1 \ n_2 \ n_3]^T \quad (5)$$

where the n_1 , n_2 and n_3 , are the direction cosine of the selected direction vector.

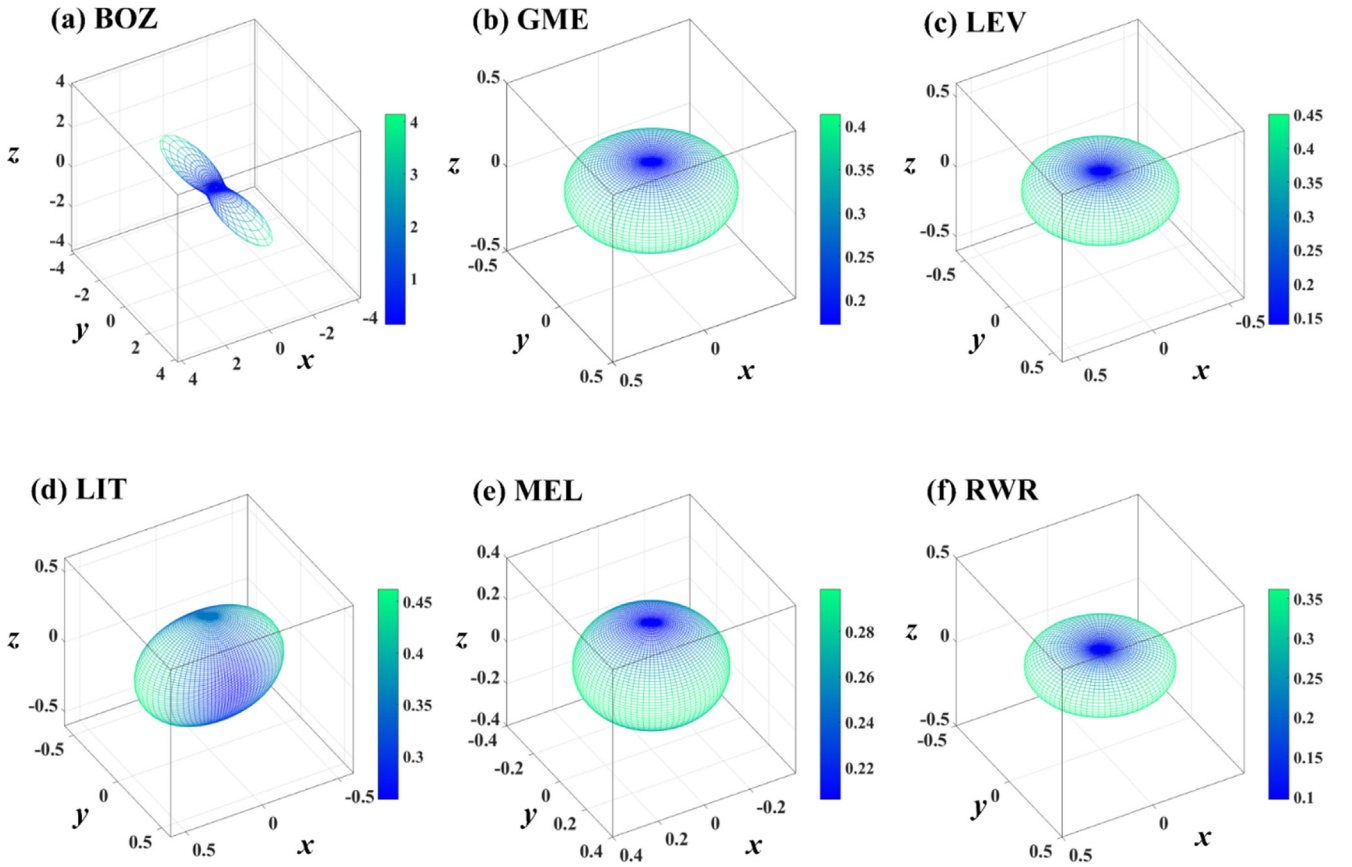
Considering only the single energy valley in the first Brillouin zone, the calculated maximum and minimum effective mass (m_{max} and m_{min}) and the ratio of m_{max}/m_{min} for the direct zeolite framework silicon allotropes are listed in Table 3. The directions of m_{max} and m_{min} are also exhibited. The directions xy and yz mean that crystals have the same effective mass in the xy plane and yz plane, which usually indicates that the material has the same transport property over the whole plane.

For electrons, ACO-Si₂₄ presents an isotropous effective mass of $0.33 m_0$, and the other allotropes are all anisotropic. BOZ-Si₉₂ has the largest electron effective mass anisotropy, and m_{max}/m_{min} of BOZ-Si₉₂ is 37.64. A lower effective mass means a higher mobility; BOZ-Si₉₂ ($0.11 m_0$), GME-Si₂₄ ($0.17 m_0$), LEV-Si₅₄ ($0.14 m_0$), LIT-Si₂₄ ($0.26 m_0$), MEL-Si₉₆ ($0.21 m_0$) and RWR-Si₃₂ ($0.10 m_0$) present lower minimum electronic effective mass than diamond silicon ($0.19 m_0$), showing the possibility of higher electronic mobility of these allotropes. Their direction-dependent effective mass of the electron is shown in Fig. 5 as three-dimensional surfaces.

For the hole effective mass, all allotropes are anisotropic, and the largest anisotropy is found in BPH-Si₂₈ and EDI-Si₅. GME-Si₂₄ shows an extremely low hole effective mass of $0.08 m_0$. AEI-Si₄₈ ($0.16 m_0$), AFX-Si₄₈ ($0.16 m_0$), BOZ-Si₉₂ ($0.15 m_0$), BPH-Si₂₈ ($0.16 m_0$), LIT-Si₂₄ ($0.12 m_0$) and SAT-Si₇₂ ($0.13 m_0$) also present lower hole effective masses than dia-

Table 3 The value and direction of the extremum of electron (m_0) and hole effective masses (m_0).

	Electron effective mass				m_{max}/m_{min}	Hole effective mass				
	m_{min}	Direction	m_{max}	Direction		m_{min}	Direction	m_{max}	Direction	m_{max}/m_{min}
ACO	0.33	–	0.33	–	1.0	0.51	(100)	0.77	(111)	1.5
AEI	0.46	(001)	0.92	(010)	2.0	0.16	(001)	0.73	(010)	4.6
AFX	0.39	(001)	0.68	xy	1.7	0.16	(001)	0.37	xy	2.3
ANA	0.43	(111)	1.00	(100)	2.3	0.61	(111)	1.40	(100)	2.3
BOZ	0.11	(001)	4.14	(010)	37.6	0.15	(010)	0.42	(023)	2.8
BPH	0.40	(001)	1.33	(100)	3.3	0.16	(100)	1.42	(001)	8.9
EDI	0.39	xy	0.56	(001)	1.4	0.27	xy	2.24	(001)	8.3
ETR	0.33	(001)	1.06	xy	3.2	0.43	(001)	0.91	xy	2.1
GME	0.17	(001)	0.41	xy	2.4	0.08	(001)	0.35	xy	4.4
LEV	0.14	(001)	0.45	xy	2.8	0.55	xy	1.56	(001)	2.8
LIT	0.26	(010)	0.46	(100)	1.8	0.12	(001)	0.62	(100)	5.2
MEL	0.21	(001)	0.30	xy	1.4	0.41	xy	0.51	(001)	1.2
RWR	0.10	(001)	0.36	xy	3.6	0.33	(001)	0.36	xy	1.1
SAT	0.37	(001)	0.62	xy	1.7	0.13	(001)	0.53	xy	4.1
SGT	0.46	(100)	0.99	xy	2.2	0.34	(001)	1.09	xy	3.2
Diamond Si	0.19	(100)	0.95	yz	5.0	0.27	(100)	0.7	(111)	2.6

**Fig. 5** Three-dimensional contour plots of electron effective masses for zeolite framework silicon allotropes with lower minimum electronic effective mass than diamond silicon.

mond silicon ($0.27 m_0$). The direction-dependent hole effective mass of hole for these six zeolite framework silicon allotropes are plotted in Fig. 6. In addition, the direction-dependent effective mass of electron and hole for other allotropes are also listed in Fig. S2 and Fig. S3, respectively.

3.4. Optical properties

In Fig. 7, the light absorption spectra under HSE06 level of the zeolite framework silicon allotropes are shown. The absorption spectrum of the d-Si and the synthesized $Cmcm$ -Si₂₄

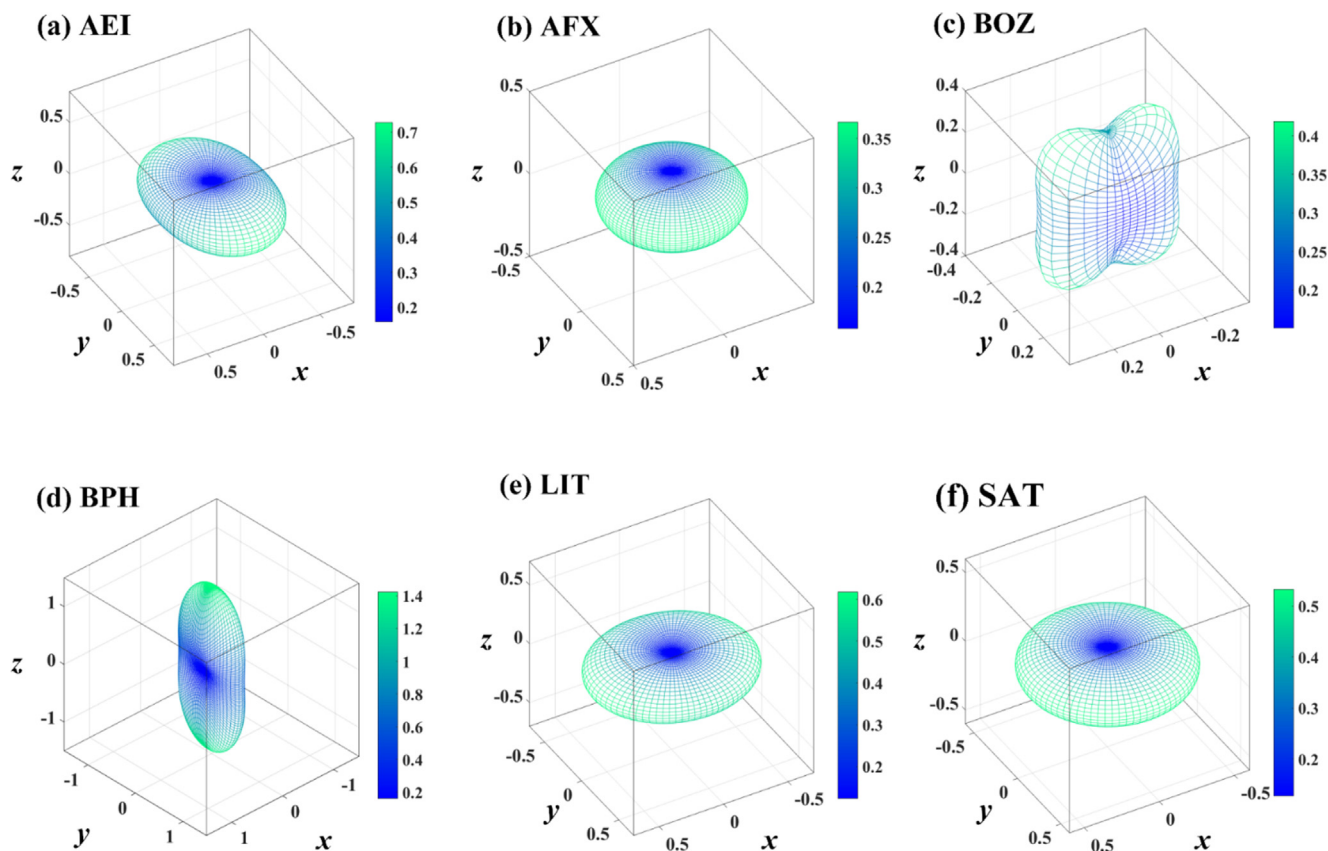


Fig. 6 Three-dimensional contour plots of hole effective masses for zeolite framework silicon allotropes with lower minimum hole effective mass than diamond silicon.

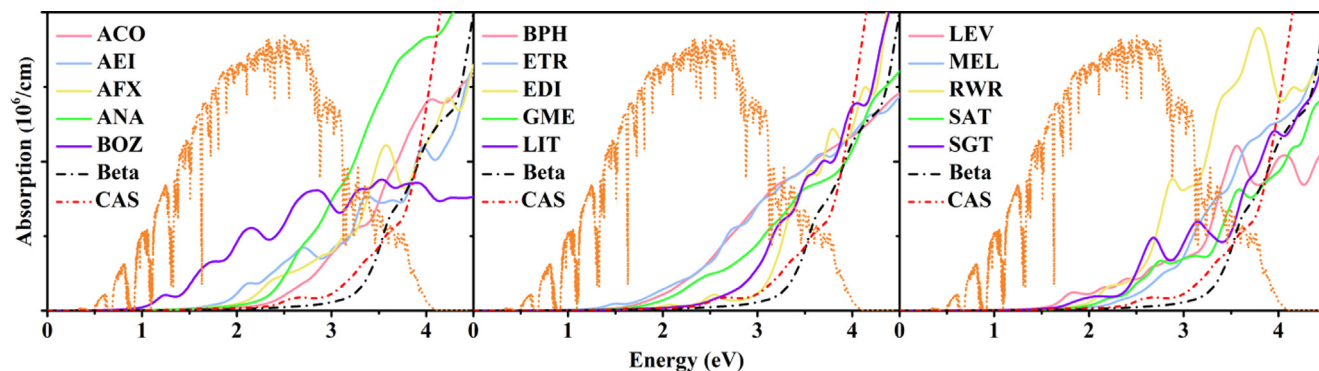


Fig. 7 Absorption spectra of selected phases. Reference air mass 1.5 solar spectral irradiance is shown in orange, whereas absorption of diamond silicon is shown in black.

(CAS-Si₂₄) is also exhibited for comparison, together with the air mass 1.5 solar spectral irradiance and visible spectrum. The main body of sunlight is visible light accompanied by a small part of infrared and ultraviolet light. These zeolite framework silicon allotropes all present higher absorption of photons in the infrared and visible region than diamond silicon and CAS-Si₂₄, especially BOZ-Si₉₂. Although BOZ-Si₉₂ with 0.47 eV direct gap does not absorb ultraviolet light well, its absorption of visible and infrared light is much higher than that of other allotropes, which is in a region perfectly compatible with the solar spectrum. ANA-Si₄₈ and RWR-Si₃₂ have

better performance under blue and ultraviolet light. Diamond silicon and CAS-Si₂₄ are both indirect band gap semiconductor, and the obvious difference of optical absorption indicates the large advantages of direct band gap silicon allotropes over indirect band gap allotropes in photovoltaic applications. Stacking several homojunction cells with different band gap together to form arrays will effectively increase the absorption efficiency of the photocell. The zeolite framework Si phases with the direct band gap in the range of 0.47 to 1.66 eV are promising materials to replace or supplement existing silicon phases.

3.5. X-ray diffraction

The simulated X-ray diffraction patterns of zeolite framework silicon allotropes are shown in Fig. 8. The strongest Bragg peak of ACO-Si₁₆, AEI-Si₄₈, AFX-Si₄₈, ANA-Si₄₈, BOZ-Si₉₂, BPH-Si₂₈, EDI-Si₅, ETR-Si₄₈, GME-Si₂₄, LEV-Si₅₄, LIT-Si₂₄, MEL-Si₉₆, RWR-Si₃₂, SAT-Si₇₂ and SGT-Si₆₄ are 011 (at 16.71 °), 110 (at 12.45 °), 011 (at 11.38 °), 112 (at 21.01 °), 130 (at 11.96 °), 010 (at 10.02 °), 010 (at 16.87 °), 111 (at 6.27 °), 010 (at 9.7 °), 012 (at 14.39 °), 020 (at 26.39 °), 101 (at 10.31 °), 004 (at 17.00 °), 101 (at 11.12 °) and 011 (at 11.79 °), respectively. The X-ray characteristics enable identification of the predicted polymorphs in future experiments.

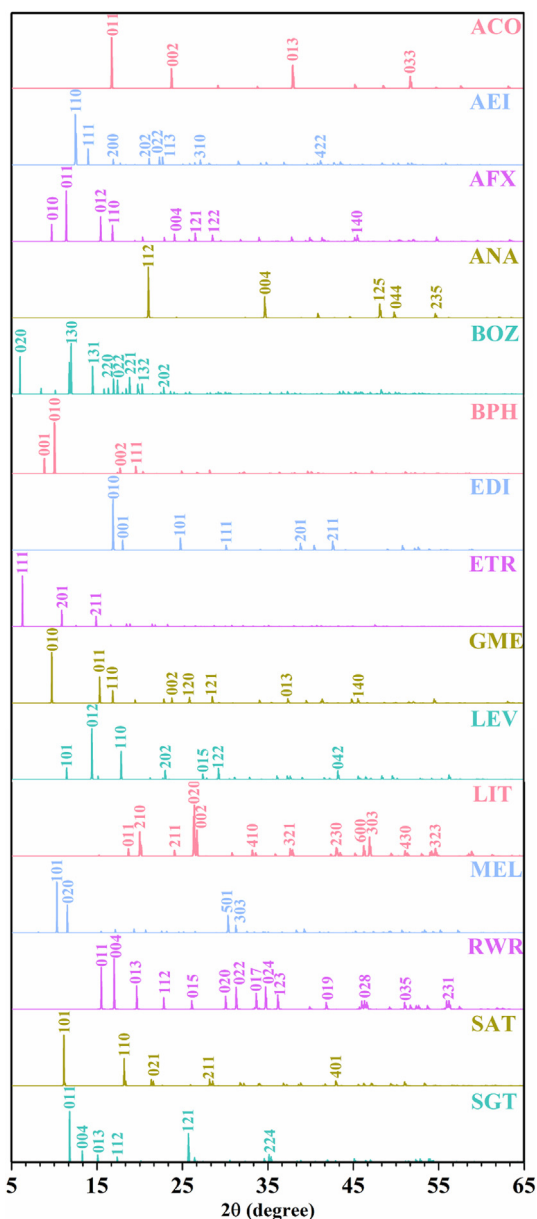


Fig. 8 X-ray diffraction patterns (Cu source with a wavelength of 1.54 Å).

4. Conclusion

We proposed fifteen zeolite framework silicon allotropes with a direct band gap of 0.47–1.66 eV. The mechanical stability and dynamic stability of the allotropes confirm that these metastable phases of silicon can exist in the ambient. These fifteen allotropes hold large cages or open channels, which generate a lower mass density. Considering that the zeolite framework silicon allotrope CAS-Si₂₄ (*CmCm*-Si₂₄) has been successfully synthesized by removing metal ions in the clathrate, these new zeolite-framework silicon allotropes with similar structural characteristics have great potential to be realized. Simulated X-ray diffraction patterns enable experimental confirmation of the predicted structures. For anisotropic properties, Young's moduli of ANA-Si₄₈ and electronic effective mass of ACO-Si₂₄ are isotropic, while Young's modulus and the carrier effective mass of the other allotropes are anisotropic. BOZ-Si₉₂ and RWR-Si₃₂ present low electron effective masses of 0.11 m_0 and 0.10 m_0 , respectively, and the lowest hole effective mass of 0.08 m_0 is found in GME-Si₂₄. For optical properties, BOZ-Si₉₂ shows especially excellent absorption of both infrared and visible photons, which makes it have a strongly potential to play a significant role as low-frequency photon absorber in tandem solar cell. Compared with conventional diamond silicon and CAS-Si₂₄, the predicted novel silicon allotropes all have higher photon absorption in the range of the solar spectrum due to their direct band gap. The direct band gap, low carrier effective mass and high photon absorption indicate that the zeolite framework silicon are promising candidates to replace diamond silicon for use in thin-film solar cell applications. Due to the large voids of the zeolite framework, the property modulation by doping guest atoms will give the zeolite framework silicon family more possibility.

Declaration of Competing Interest

The authors declare that they have no known competing financial interests or personal relationships that could have appeared to influence the work reported in this paper.

Acknowledgements

This work was supported by the National Natural Science Foundation of China (No. 61974116); the National Natural Science Foundation of China (No. 61804120)

Appendix A. Supplementary material

Supplementary data to this article can be found online at <https://doi.org/10.1016/j.arabjc.2022.104377>.

References

- Ackland, G.J., 2001. Theory of high pressure phases of Group-IV and III-V semiconductors. *Rep. Prog. Phys.* 223, 361–368. [https://doi.org/10.1002/1521-3951\(200101\)223:2<361::Aid-Pssb361>3.0.Co;2-1](https://doi.org/10.1002/1521-3951(200101)223:2<361::Aid-Pssb361>3.0.Co;2-1).
- Amsler, M., Botti, S., Marques, M.A.L., Lenosky, T.J., Goedecker, S., 2015. Low-density silicon allotropes for photovoltaic applications. *Phys. Rev. B* 92, <https://doi.org/10.1103/PhysRevB.92.014101> 014101.
- Baerlocher, C., L. B. McCusker and D. H. Olson, 2007. *Atlas of Zeolite Framework Types*, Elsevier: Amsterdam. <https://doi.org/10.1016/B978-0-444-53064-6.X5186-X>.
- Besson, J.M., Mokhtari, E.H., Gonzalez, J., Weill, G., 1987. Electrical properties of semimetallic silicon III and semiconductive silicon IV at ambient pressure. *Phys. Rev. Lett.* 59, 473–476. <https://doi.org/10.1103/PhysRevLett.59.473>.
- Botti, S., Flores-Livas, J.A., Amsler, M., Goedecker, S., Marques, M. A.L., 2012. Low-energy silicon allotropes with strong absorption in

- the visible for photovoltaic applications. *Phys. Rev. B* 86,. <https://doi.org/10.1103/PhysRevB.86.121204> 121204.
- Fan, Q., Chai, C., Wei, Q., Yan, H., Zhao, Y., Yang, Y., Yu, X., Liu, Y., Xing, M., Zhang, J., Yao, R., 2015. Novel silicon allotropes: stability, mechanical, and electronic properties. *J. Appl. Phys.* 118,. <https://doi.org/10.1063/1.4935549> 185704.
- Fan, Q., Chai, C., Wei, Q., Yang, Y., 2016. Two novel silicon phases with direct band gaps. *Phys. Chem. Chem. Phys.* 18, 12905–12913. <https://doi.org/10.1039/c6cp00195e>.
- Fan, Q., Niu, R., Zhang, W., Zhang, W., Ding, Y., Yun, S., 2019. t-Si64: a novel silicon allotrope. *Chemphyschem.* 20, 128–133. <https://doi.org/10.1002/cphc.201800903>.
- Fan, Q., Li, C., Yang, R., Yu, X., Zhang, W., Yun, S., 2021. Stability, mechanical, anisotropic and electronic properties of σ P8 carbon: a superhard carbon allotrope in orthorhombic phase. *J. Solid State Chem.* 294,. <https://doi.org/10.1016/j.jssc.2020.121894> 121894.
- Fan, Q., Wu, N., Yang, R., Zhang, W., Yu, X., Yun, S., 2022. All sp² hybridization BN polymorphs with wide bandgap. *J. Appl. Phys.* 131,. <https://doi.org/10.1063/5.0069491> 055703.
- Fix, T., Vollandat, R., Ameer, A., Roques, S., Rehspringer, J.-L., Chevalier, C., Muller, D., Slaoui, A., 2020. Silicon clathrate films for photovoltaic applications. *J. Phys. Chem. C* 124, 14972–14977. <https://doi.org/10.1021/acs.jpcc.0c02712>.
- Guerette, M., Ward, M.D., Zhu, L., Strobel, T.A., 2020. Single-crystal synthesis and properties of the open-framework allotrope Si₂₄. *J. Phys-Condens. Matter* 32,. <https://doi.org/10.1088/1361-648X/ab699d> 194001.
- Guo, Y., Wang, Q., Kawazoe, Y., Jena, P., 2015. A new silicon phase with direct band gap and novel optoelectronic properties. *Sci. Rep.* 5, 14342. <https://doi.org/10.1038/srep14342>.
- Hafner, J., 2008. Ab-initio simulations of materials using VASP: Density-functional theory and beyond. *J. Comput. Chem.* 29, 2044–2078. <https://doi.org/10.1002/jcc.21057>.
- He, C., Shi, X., Clark, S.J., Li, J., Pickard, C.J., Ouyang, T., Zhang, C., Tang, C., Zhong, J., 2018. Complex low energy tetrahedral polymorphs of Group IV elements from first principles. *Phys. Rev. Lett.* 121,. <https://doi.org/10.1103/PhysRevLett.121.175701> 175701.
- Hohenberg, P., Kohn, W., 1964. Inhomogeneous electron gas. *Phys. Rev.* 136, B864–B871. <https://doi.org/10.1103/PhysRev.136.B864>.
- Hu, M., Wang, Z., Xu, Y., Liang, J., Li, J., Zhu, X., 2018. fvs-Si₄₈: a direct bandgap silicon allotrope. *Phys. Chem. Chem. Phys.* 20, 26091–26097. <https://doi.org/10.1039/c8cp03165g>.
- Jamieson, J.C., 1963. Crystal structures at high pressures of metallic modifications of Silicon and Germanium. *Science* 139, 762–764. <https://doi.org/10.1126/science.139.3556.762>.
- Jiao, N., Zhou, P., He, C., He, J., Liu, X., Sun, L., 2019. Low-energy GeP monolayers with natural type-II homojunctions for SunLight-driven water splitting. *Phys. Status Solidi-R* 13, 1900470. <https://doi.org/10.1002/pssr.201900470>.
- Kohn, W., Sham, L.J., 1965. Self-consistent equations including exchange and correlation effects. *Phys. Rev.* 140, A1133–A1138. <https://doi.org/10.1103/PhysRev.140.A1133>.
- Krukau, A.V., Vydrov, O.A., Izmaylov, A.F., Scuseria, G.E., 2006. Influence of the exchange screening parameter on the performance of screened hybrid functionals. *J. Chem. Phys.* 125,. <https://doi.org/10.1063/1.2404663> 224106.
- Malone, B.D., Sau, J.D., Cohen, M.L., 2008. Ab initio study of the optical properties of Si-XII. *Phys. Rev. B* 78,. <https://doi.org/10.1103/PhysRevB.78.161202> 161202.
- Malone, B.D., Sau, J.D., Cohen, M.L., 2008. Ab initio survey of the electronic structure of tetrahedrally bonded phases of silicon. *Phys. Rev. B* 78,. <https://doi.org/10.1103/PhysRevB.78.035210> 035210.
- Mujica, A., Rubio, A., Muñoz, A., Needs, R.J., 2003. High-pressure phases of group-IV, III–V, and II–VI compounds. *Rev. Mod. Phys.* 75, 863–912. <https://doi.org/10.1103/RevModPhys.75.863>.
- O’Keeffe, M., Peskov, M.A., Ramsden, S.J., Yaghi, O.M., 2008. The reticular chemistry structure resource (RCSR) database of, and symbols for, crystal nets. *Acc. Chem. Res.* 41, 1782–1789. <https://doi.org/10.1021/ar800124u>.
- Ouyang, T., Cui, C., Shi, X., He, C., Li, J., Zhang, C., Tang, C., Zhong, J., 2020. Systematic enumeration of low-energy graphyne allotropes based on a coordination-constrained searching strategy. *Phys. Status Solidi-R* 14, 2000437. <https://doi.org/10.1002/pssr.202000437>.
- Shi, X., He, C., Pickard, C.J., Tang, C., Zhong, J., 2018. Stochastic generation of complex crystal structures combining group and graph theory with application to carbon. *Phys. Rev. B* 97,. <https://doi.org/10.1103/PhysRevB.97.014104> 014104.
- Shiell, T.B., Strobel, T.A., 2020. Compression of sodium-filled and empty open-framework Si₂₄ under quasihydrostatic and nonhydrostatic conditions. *Phys. Rev. B* 102,. <https://doi.org/10.1103/PhysRevB.102.094107> 094107.
- Song, Y., Chai, C., Fan, Q., Zhang, W., Yang, Y., 2019. Physical properties of Si-Ge alloys in C_{2/m} phase: a comprehensive investigation. *J. Phys-Condens. Mat.* 31,. <https://doi.org/10.1088/1361-648X/ab11a2> 255703.
- Song, Y., Chai, C., Fan, Q., Zhang, W., Yang, Y., 2020. Effective mass anisotropy of Si-Ge alloys: a discussion of the effective mass tensor. *Phys. Scripta* 95,. <https://doi.org/10.1088/1402-4896/abbde1> 115808.
- Stefano, B., G. Stefano de, C. Andrea Dal and G. Paolo, 2001. Phonons and related crystal properties from density-functional perturbation theory. *Rev. Mod. Phys.* 73, 515. <https://doi.org/10.1103/RevModPhys.73.515>
- Su, L., Li, S., Li, J., He, C., Zeng, X.-T., Sheng, X.-L., Ouyang, T., Chunxiao, Z., Tang, C., Zhong, J., 2022. I4/mcm-Si₄₈: an ideal topological nodal-line semimetal. *ACS Mater. Lett.* 4, 1726–1733. <https://doi.org/10.1021/acsmaterialslett.2c00333>.
- Togo, A., Tanaka, I., 2015. First principles phonon calculations in materials science. *Scripta Mater.* 108, 1–5. <https://doi.org/10.1016/j.scriptamat.2015.07.021>.
- Wang, Q., Xu, B., Sun, J., Liu, H., Zhao, Z., Yu, D., Fan, C., He, J., 2014. Direct band gap silicon allotropes. *J. Am. Chem. Soc.* 136, 9826–9829. <https://doi.org/10.1021/ja5035792>.
- Wei, Y., Li, J., Shi, X., Li, J., He, C., 2022. First-principles study on the electronic, mechanical and optical properties for silicon allotropes in hexagonal 2–7 stacking orders. *Scripta Mater.* 219,. <https://doi.org/10.1016/j.scriptamat.2022.114843> 115808.
- Wei, Q., Tong, W., Wei, B., Zhang, M., Peng, X., 2019. Six new silicon phases with direct band gaps. *Phys. Chem. Chem. Phys.* 21, 19963–19968. <https://doi.org/10.1039/c9cp03128f>.
- Wippermann, S., He, Y., Vörös, M., Galli, G., 2016. Novel silicon phases and nanostructures for solar energy conversion. *Appl. Phys. Rev.* 3,. <https://doi.org/10.1063/1.4961724> 040807.
- Yang, X., He, C., Shi, X., Li, J., Zhang, C., Tang, C., Zhong, J., 2018. First-principles prediction of two hexagonal silicon crystals as potential absorbing layer materials for solar-cell application. *J. Appl. Phys.* 124,. <https://doi.org/10.1063/1.5046560> 163107.
- Zhang, D., Niu, H., Li, Y., Huang, H.-M., Jiang, P., Li, Y.-L., 2021. Tuning of electronic and optical properties of a predicted silicon allotrope: hexagonal silicon h_{10} -Si. *Phys. Rev. B* 104,. <https://doi.org/10.1103/PhysRevB.104.125201> 125201.